Computer Physics Communications 222 (2018) 46–58

Contents lists available at ScienceDirect

Computer Physics Communications

journal homepage: www.elsevier.com/locate/cpc

Reliability of the time splitting Fourier method for singular solutions in quantum fluids

M. Caliari *, S. Zuccher

Department of Computer Science, University of Verona, Strada Le Grazie 15, 37134 Verona, Italy

ARTICLE INFO

Article history:
Received 29 December 2016
Received in revised form 1 September 2017
Accepted 15 September 2017
Available online 28 September 2017

Keywords:
Quantum fluids
Gross–Pitaevskii equation
Nonlinear Schrödinger equation
Nonuniform finite differences
Time splitting
Fourier spectral method

ABSTRACT

We study the numerical accuracy of the well-known time splitting Fourier spectral method for the approximation of singular solutions of the Gross–Pitaevskii equation. In particular, we explore its capability of preserving a steady-state vortex solution, whose density profile is approximated by an accurate diagonal Padé expansion of degree [8, 8], here explicitly derived for the first time. We show by several numerical experiments that the Fourier spectral method is only slightly more accurate than a time splitting finite difference scheme, while being reliable and efficient. Moreover, we notice that, at a post-processing stage, it allows an accurate evaluation of the solution outside grid points, thus becoming particularly appealing for applications where high resolution is needed, such as in the study of quantum vortex interactions.

1. Introduction

Quantum turbulence [1–3], as well as classical turbulence [4,5], is dominated by reconnection of vortical structures which is much simpler to treat in the framework of quantum fluids rather than in viscous fluids [6], while leading to similar features such as time asymmetry [7]. Despite the fundamental differences between the two forms of turbulence, there are reasons to believe that the understanding of quantum turbulence might shed new light on the understanding of its classical counterpart [3].

Quantum fluid dynamics is properly described by a nonlinear Schrödinger equation which, in this framework, takes the name of Gross–Pitaevskii equation (GPE) [8,9]

$$\frac{\partial \psi}{\partial t} = \frac{\mathrm{i}}{2}\nabla^2\psi + \frac{\mathrm{i}}{2}\left(1 - |\psi|^2\right)\psi, \tag{1}$$

where ψ is the complex wave function. The derivation of the above equation as a model of superfluidity can be found, for instance, in [10,11]. Through the Madelung transformation $\psi = \sqrt{\rho}\,\exp(\mathrm{i}S)$ and $\boldsymbol{u} = \nabla S$, Eq. (1) can be stated also in classical fluid dynamical terms. Defects in the wave function ψ are interpreted as infinitesimally thin vortices of constant circulation $\Gamma = \oint \boldsymbol{u}\cdot\mathrm{d}\boldsymbol{s} = 2\pi$, with healing length ξ equal to 1, which implies $\lim_{|x|\to\infty}|\psi(t,x)| = 1$.

Another form of the Gross–Pitaevskii equation, which is used to model Bose–Einstein Condensates (BECs) with vanishing boundary conditions, includes a space dependent trapping potential V

$$\mathrm{i}\frac{\partial \Psi}{\partial t} = -\frac{1}{2}\nabla^2\Psi + V\Psi + \beta|\Psi|^2\Psi, \quad \lim_{|x|\to\infty}|\Psi(t,x)| = 0,$$

where $\beta > 0$ is the so-called coupling constant. We refer the reader to [12] for a review of the mathematical theory and numerical methods for BECs.

In the framework of quantum fluids, the main reason for preferring the GPE approach to others for the study of quantum turbulence is that it guarantees a natural dynamics of interacting vortices [13] while resolving fine scales up to the vortex core [3,14]. On the contrary, methods based on the inviscid Euler equations (either their direct numerical simulation [15] or vortex filament methods [16]) are unable to automatically perform vortex reconnections, being forbidden by Euler dynamics.

* Corresponding author.
E-mail addresses: marco.caliari@univr.it (M. Caliari), simone.zuccher@univr.it (S. Zuccher).

https://doi.org/10.1016/j.cpc.2017.09.013
0010-4655/

The numerical solution of the GPE (1) is normally carried out by employing time splitting Fourier methods [7,13,17–19] and by imposing vortices in a unitary background density, i.e. $\rho_\infty = |\psi_\infty|^2 = 1$. However, these methods assume periodic boundary conditions. Solutions which are not periodic must be mirrored in the directions lacking periodicity [17], thus imposing doubling of the degrees of freedom in each of those directions and a consequent increase of the computational effort.

Recent developments [13,19,20] have shown that reconnections in quantum fluids are strictly related to topological features characterizing the interacting vortex tubes such as writhe, total torsion and intrinsic twist. These quantities depend on the fine details of the curve that describes the vortex centerline (its third derivative with respect to the curvilinear abscissa is required for computing torsion) and on the phase of the wave function ψ in the neighborhood of the vortex centerline. In [21] the pseudo-vorticity field is used to track the topological defects of the superfluid and reconstruct the vortex centerlines which correspond to zeros of the field. Moreover, by assuming a periodic field, Fourier representation is exploited to retain spectral accuracy for both the wave function and its derivatives, so as to accurately compute curvature and torsion. Other works [22,23] have tackled the issue of tracking in an accurate and reliable way vortices whose dynamics is prescribed by the Gross–Pitaevskii model. Therefore it is paramount to resort to high resolution numerical simulations of Eq. (1), especially in the proximity of the reconnection event.

With the goal of assessing the goodness of time-splitting Fourier methods for singular solutions on uniform grids versus time-splitting finite differences on nonuniform grids, we focus on the two-dimensional straight vortex, which is the prototype commonly employed for more complex vortex geometries, such as vortex rings and vortex knots [13,19,20]. We first derive an analytical approximation of the steady state vortex that nullifies the right-hand-side of (1). Then we perform a systematic comparison between the two approaches by measuring the deviation of the numerical solution from the initial condition (being steady the initial condition should remain preserved). Finally, we explore the possibility to evaluate the solution obtained by time-splitting Fourier methods on nonuniform grids designed to guarantee higher spatial resolution in the proximity of vortex singularity. Both time-splitting Fourier and finite differences methods can be easily extended to the three-dimensional case, in which they preserve their properties.

2. Accurate Padé approximation of a 2d vortex

In this section, we seek an analytical approximation of the two-dimensional, steady-state solution of Eq. (1) that represents a straight vortex centered at the origin in a constant background density ρ_∞ and compare it to the numerical solution obtained by finite differences.

It is well-known that the classical two-dimensional Euler vortex of circulation Γ has azimuthal velocity $u_\theta = \Gamma/(2\pi r)$ where $r = \sqrt{x_1^2 + x_2^2}$ is the radius and $\theta = \operatorname{atan2}(x_2, x_1) = \arg(x_1 + \mathrm{i}x_2) \in (-\pi, \pi]$ is the azimuthal angle. It should be noted that $u_\theta \to 0$ at infinity and $u_\theta \to \infty$ for $r \to 0$. The cartesian components of the velocity are thus $u_1 = -u_\theta \sin\theta = -\Gamma x_2/(2\pi r^2)$ and $u_2 = u_\theta \cos\theta = \Gamma x_1/(2\pi r^2)$. Therefore $\boldsymbol{u} = (u_1, u_2) = (\Gamma/(2\pi))\nabla\theta$. This shows that the velocity field is solenoidal ($\nabla \cdot \boldsymbol{u} = 0$), that the quantum mechanical phase, S, is simply the azimuthal angle θ, and that the quantum of circulation, in our dimensionless units, is equal to 2π. In steady conditions, the continuity equation ensures that $\nabla \cdot (\rho \boldsymbol{u}) = 0$, hence $\boldsymbol{u} \cdot \nabla\rho = 0$, which means that $\nabla\rho \cdot \nabla\theta = 0$. The solution $\rho \equiv \bar\rho$, $\bar\rho \neq 0$, uniform in space would result in atoms moving at infinite speed on the vortex center $r = 0$. The other possibility is that $\nabla\rho \perp \nabla\theta$. Since $\nabla\theta = \hat\theta/r$, then $\nabla\rho$ is parallel to $\hat r$ and thus $\rho = \rho(r)$, $\hat r$ and $\hat\theta$ being the unitary vectors in two-dimensional polar coordinates.

In a two-dimensional domain we set $\psi(x_1, x_2) = \rho(\sqrt{x_1^2 + x_2^2})^{1/2} \mathrm{e}^{\mathrm{i}\theta(x_1,x_2)}$ where $\rho(\sqrt{x_1^2 + x_2^2}) = \rho(r)$ is a function to be determined. By imposing that ψ is the steady solution of Eq. (1), we find that ρ satisfies the equation

$$\rho'' + \frac{\rho'}{r} - \frac{(\rho')^2}{2\rho} - \frac{2\rho}{r^2} + 2(1-\rho)\rho = 0, \tag{2}$$

with boundary conditions $\rho(0) = 0$ and $\rho(\infty) = 1$, which is the only admissible constant background density.

It is known [11,24] that Padé approximations of $\rho(r)$ retain only even degrees at both the numerator and denominator, that is

$$\rho(r) \approx \frac{\sum_{j=0}^{p} a_j r^{2j}}{1 + \sum_{k=1}^{q} b_k r^{2k}} = \frac{a_0 + a_1 r^2 + a_2 r^4 + \cdots + a_p r^{2p}}{1 + b_1 r^2 + b_2 r^4 + \cdots + b_q r^{2q}}. \tag{3}$$

In order for this approximation to satisfy the boundary conditions, it must be

$$\rho(0) = 0 \Longrightarrow a_0 = 0$$
$$\rho(\infty) = 1 \Longrightarrow p = q, \quad b_q = a_p.$$

Given these simplifications, the diagonal Padé approximation, with $2q - 1$ coefficients and both numerator and denominator of degree r^{2q}, is

$$\rho_q(r) = \frac{a_1 r^2 + a_2 r^4 + a_3 r^6 + \cdots + a_q r^{2q}}{1 + b_1 r^2 + b_2 r^4 + b_3 r^6 + \cdots + a_q r^{2q}}. \tag{4}$$

In literature this approximation is normally limited to $q = 2$ [11], that is

$$\rho_2(r) = \frac{a_1 r^2 + a_2 r^4}{1 + b_1 r^2 + a_2 r^4}$$

with

$$a_1 = \frac{11}{32}, \quad b_1 = \frac{5 - 32a_1}{48 - 192a_1}, \quad a_2 = a_1\left(b_1 - \frac{1}{4}\right).$$

Despite its widespread usage, this approximation is qualitatively wrong because it reaches a maximum above $\rho(\infty) = 1$ (see insert in Fig. 1) at $\bar r = 2\sqrt{6\left(4 + 3\sqrt{2}\right)} \approx 14.065$, unique positive solution of $r^4 - 192r^2 - 1152$ obtained by imposing $\rho_2'(r) = 0$. The solution of Eq.

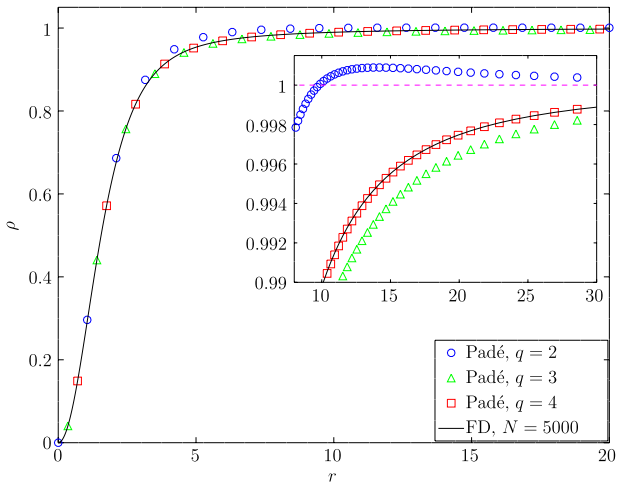

Fig. 1. Comparison between $\left[\tilde{g}\left(\frac{r}{1+r}\right)\right]^2$, numerical solution of (7) obtained by second-order finite differences on 5000 equispaced points, and different Padé approximations $\rho_q(r)$.

(2) cannot have a maximum above 1, corresponding to $\rho'(\bar{r}) = 0$, because the second derivative

$$\rho''(\bar{r}) = \frac{2\rho(\bar{r})}{\bar{r}^2} + 2(\rho(\bar{r}) - 1)\rho(\bar{r})$$

would be positive.

Due to these limitations, we seek higher-order ($q > 2$), Padé expansions, namely

$$\rho_3(r) = \frac{a_1 r^2 + a_2 r^4 + a_3 r^6}{1 + b_1 r^2 + b_2 r^4 + a_3 r^6} \quad \text{and} \quad \rho_4(r) = \frac{a_1 r^2 + a_2 r^4 + a_3 r^6 + a_4 r^8}{1 + b_1 r^2 + b_2 r^4 + b_3 r^6 + a_4 r^8}.$$

In order to determine the coefficients of a certain approximation $\rho_q(r)$, we compute the analytical expressions $\rho_q(r)$, $\rho_q'(r)$ and $\rho_q''(r)$ and substitute them in Eq. (2) obtaining the form

$$\rho_q'' + \frac{\rho_q'}{r} - \frac{(\rho_q')^2}{2\rho_q} - \frac{2\rho_q}{r^2} + 2(1 - \rho_q)\rho_q = 0 \iff \frac{N_q(r)}{D_q(r)} = 0. \tag{5}$$

The numerator $N_q(r)$ is made of terms r^{2k}, which are in a number much larger than the $2q - 1$ degrees of freedom of the Padé expansion. For this reason Eq. (2) cannot be satisfied exactly. However, we can nullify the coefficients of $2q - 1$ terms r^{2k}. We can choose to start from higher- or lower-order coefficients in $N_q(r)$. We prefer to operate on lower-order powers of r^{2k}, i.e. $k = 1, \ldots, 2q - 1$, because we need a good approximation of $\rho_q(r)$ in a neighborhood of the origin. Interestingly enough, we observe *a posteriori* that canceling the lower-order coefficients of r^{2k} results in very small values of the coefficients of larger powers of r. The step-by-step derivation of $\rho_q(r)$ for $q = 2, 3, 4$ is reported in Appendix, whereas Tables A.1 and A.2 summarize all coefficients for the expansions ρ_q, $q = 2, 3, 4$.[1]

In order to test the reliability of these approximations, we compare them with a numerical solution. In this case, it is more convenient to compute directly $f(r) = \rho(r)^{1/2}$, as first suggested by [17], which satisfies

$$f'' + \frac{f'}{r} + f\left(1 - f^2 - \frac{1}{r^2}\right) = 0 \tag{6}$$

with $f(0) = 0$ and $f(\infty) = 1$.

Eq. (6) could be integrated numerically as it is, by artificially bounding the infinite domain. To avoid this problem, we resort to the change of variables $s = r/(1 + r)$, $g(s) = f(r)$, which yields the equation for $g(s)$

$$(s-1)^4 g'' + 2(s-1)^3 g' - \frac{(s-1)^3}{s} g' - \frac{(s-1)^2}{s^2} g + (1 - g^2)g = 0, \tag{7}$$

defined in the finite domain $s \in (0, 1]$, with boundary conditions $g(0) = 0$ and $g(1) = 1$. We solve Eq. (7) by central second order finite differences with equally spaced discretization points $s_i = i/N$, $i = 1, 2, \ldots, N$. Given the numerical solution $\tilde{g}$ of (7), the numerical approximation of the density is

$$\rho_{\text{num}}(r_i) = \left[\tilde{g}\left(\frac{r_i}{1 + r_i}\right)\right]^2 \tag{8}$$

where $r_i = s_i/(1 - s_i)$, $i = 1, 2, \ldots, N - 1$. This rescaling provides denser points r_i in the neighborhood of the origin, where they are mostly needed (more than 95% of the points r_i are in the interval $0 \le r \le 20$). Nevertheless, the computation of the initial solution for (1) on a two-dimensional grid, for instance, requires ρ_{num} to be interpolated.

[1] The SageMath code for the computation of the coefficients is available on request by contacting the corresponding author.

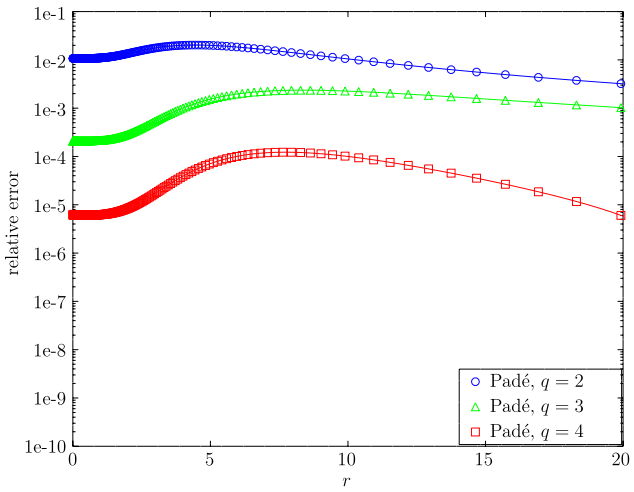

Fig. 2. Relative error (for $r \neq 0$) between different Padé approximations $\rho_q(r)$ and the numerical solution of (7) obtained by second-order finite differences on 5000 equispaced points.

In Fig. 1 we show the comparison between the numerical solution of (7) by employing second-order central finite differences with 5000 points and different Padé approximations $\rho_q(r)$ for $q = 2, 3, 4$. Visual inspection confirms that $q = 2$ is a poor representation of the solution of Eq. (2), especially for $4 < r < 20$.

To appreciate quantitatively the error with respect to the numerical solution, in Fig. 2 we report the relative error in a semilog plot. We observe that in general the relative error decreases for increasing order of Padé approximation. In particular for $r \to 0$, $\rho_4(r)$ exhibits the profile that better fits the numerical solution. Finally, the first derivatives ρ_3' and ρ_4' are always positive, i.e. no overshooting is observed.

3. Time splitting methods

Here we introduce the Strang splitting methods for the Gross–Pitaevskii equation, in which the kinetic linear part is solved either by the Fourier spectral method or nonuniform finite differences.

As we have seen above, the Gross–Pitaevskii equation has been extensively employed not only for simulating the dynamics of vortices in a uniform background density but also for BECs with vanishing boundary conditions [12]

$$\lim_{|x|\to\infty} |\Psi(t,x)| = 0.$$

It is easy to prove that such conditions lead to the preservation of the total mass in any dimension d

$$\int_{\mathbb{R}^d} |\Psi(t,x)|^2 \mathrm{d}x,$$

where $x = (x_1, \ldots, x_d)$. In fact, over a bounded domain $\Omega \subset \mathbb{R}^d$ with boundary S

$$\begin{aligned} \frac{\mathrm{d}}{\mathrm{d}t}\int_\Omega |\Psi(t,x)|^2 \mathrm{d}x &= \int_\Omega \left(\frac{\partial \Psi(t,x)}{\partial t}\overline{\Psi}(t,x) + \frac{\partial \overline{\Psi}(t,x)}{\partial t}\Psi(t,x) \right) \mathrm{d}x = \\ &= \frac{\mathrm{i}}{2}\int_S \left(\overline{\Psi}(t,x)\nabla\Psi(t,x)\cdot\vec{n} - \Psi(t,x)\nabla\overline{\Psi}(t,x)\cdot\vec{n} \right) \mathrm{d}S, \end{aligned} \tag{9}$$

thus the derivative of the mass tends to zero as Ω tends to $\mathbb{R}^d$. In the case of vanishing boundary conditions, widely used schemes for the numerical simulation of the dynamics of (1) are the so-called time-splitting pseudospectral/finite difference methods and the finite difference time domain methods (see [12] for a review). If we restrict the options to second-order accurate schemes in time, Time Splitting pseudoSPectral (TSSP) methods, Time Splitting Finite Difference (TSFD) methods and Crank–Nicolson Finite Difference (CNFD) method conserve the mass at the discretized level when periodic, homogeneous Dirichlet or homogeneous Neumann boundary conditions are imposed in the bounded domain of discretization. We refer the reader to [25] for higher-order time splitting methods.

When studying the evolution of bright-tailed structures such as the two-dimensional vortices described above, homogeneous Dirichlet boundary conditions are not compatible and must be excluded. Periodic boundary conditions and Fourier spectral decomposition can be used after a proper mirroring of the computational domain (see Section 3.1). Homogeneous Neumann boundary conditions can be used and are easy to implement for Finite Difference schemes in space. As a side effect, both periodic and homogeneous Neumann boundary conditions preserve the mass over bounded domains, since the boundary term in (9) vanishes. From the time discretization point of view, CNFD is implicit and requires the solution of a coupled nonlinear system at each time step. For this reason we resorted to time splitting methods.

In [12, Example 4.1] TSSP is suggested when the solution is smooth and TSFD otherwise, although the hint comes from a one-dimensional numerical experiment. In what follows, we analyze two approaches: a classical time splitting Fourier method and a time

splitting *nonuniform* finite difference method. In any case, equation (1) is split into two parts

$$\frac{\partial u}{\partial t}(t,x) = \frac{\mathrm{i}}{2}\nabla^2 u(t,x) \tag{10a}$$

$$\frac{\partial v}{\partial t}(t,x) = \frac{\mathrm{i}}{2}\left(1-|v(t,x)|^2\right)v(t,x). \tag{10b}$$

The solution of the first equation depends on the space chosen for the discretization and will be described in the next two sections. The second equation can be solved exactly, taking into account that $|v|$ is preserved by the equation. Therefore

$$v(\tau,x) = \exp\left(\frac{\tau\mathrm{i}}{2}\left(1-|v(0,x)|^2\right)\right)v(0,x) \tag{11}$$

for any x in the spatial domain. If we denote by $\mathrm{e}^{\tau\mathcal{A}}u_n(x)$ and $\mathrm{e}^{\tau\mathcal{B}(v_n(x))}v_n(x)$ the two partial numerical solutions, the approximation $\psi_{n+1}(x)$ of $\psi(t_{n+1},x)$, where $t_{n+1}=(n+1)\tau$, can be recovered by the so-called Strang splitting

$$\psi_{n+1/2}(x) = \mathrm{e}^{\tau\mathcal{A}}\mathrm{e}^{\frac{\tau}{2}\mathcal{B}(\psi_n(x))}\psi_n(x)$$

$$\psi_{n+1}(x) = \mathrm{e}^{\frac{\tau}{2}\mathcal{B}(\psi_{n+1/2}(x))}\psi_{n+1/2}(x).$$

3.1. Time splitting Fourier method

Eq. (10a) can be solved exactly in time within the Fourier spectral space. Apart from the error at machine-precision level coming from the necessary direct and inverse Fast Fourier Transforms (FFTs), the only possible considerable error might arise from an insufficient number of Fourier modes. This is usually not a big deal when approximating smooth solutions fast decaying to zero, since spectral order of convergence takes place. For this to happen, the unbounded domain has to be truncated to a computational bounded domain Ω large enough to support the most of a periodic approximation of the solution. However, when simulating the dynamics of vortex solutions not decaying to zero, as in our case where $\lim_{|x|\to\infty}|\psi(t,x)|=1$, the main issue is the lack of periodicity at the boundaries. This can be overcome by introducing mirror vortices in those directions [17], with the consequent increase of the computational effort due to the doubling the degrees of freedom in each of those directions. Such a mirroring, however, does not make the initial solution truly periodic as it guarantees the same values, at opposite boundaries, only for ψ and not for its derivatives. A similar situation appears in [26], where an ansatz wave function for a system of superfluid vortices in a periodic two-dimensional square is presented. In that case, the values of ψ are periodic through a modification of its phase at the boundaries. As far as the regularity of the solution in the neighborhood of the vortex core is concerned, it should be noted that the phase field has a singularity in the vortex position, whereas the density goes smoothly to zero keeping the wave function nonsingular.

In order to investigate the accuracy of Fourier approximation for vortex solutions, we consider the Fourier series expansion of the function obtained by mirroring

$$\psi_0(r,\theta) = \rho_4^{1/2}(r)\mathrm{e}^{\mathrm{i}\theta}, \quad \psi_0 : [-L,L)^2 \to \mathbb{C} \tag{12a}$$

and

$$\psi_0^\eta(r,\theta) = \rho_4^{1/2}(r)\mathrm{e}^{\mathrm{i}\theta}\eta(r), \quad \psi_0^\eta : [-L,L)^2 \to \mathbb{C} \tag{12b}$$

with respect to the axis $x=L$ and $y=L$, where $\eta(r)$ is the mollifier

$$\eta(r) = \begin{cases} \mathrm{e}^{1-\frac{1}{1-(r/L)^2}} & \text{for } 0 \le r < L, \\ 0 & \text{elsewhere.} \end{cases}$$

The mollifier $\eta(r)$ preserves the shape of the density and the phase defect at the origin and make ψ_0^η to vanish with all its derivatives towards $r=L$. The final computational domain is $\Omega=[-L,3L)^2$, with $L=20$. We compute a reference approximation by an expansion into a series with $(2\cdot 2048)^2$ Fourier modes and compare it with expansions ranging between $M=m^2=(2\cdot 32)^2$ and $M=m^2=(2\cdot 512)^2$ modes, in the L^2 norm. For the mollified ψ_0^η we observe in Fig. 3 a typical spectral rate of convergence, while for the original ψ_0 wave function representing the straight vortex we observe a strong order reduction (the observed rate of convergence is roughly 3/2). We conclude that spectral accuracy is not reached because the solution at the boundaries in not truly periodic with all its derivatives. The phase singularity at the vortex position does not affect spectral convergence.

Increasing the number of Fourier coefficients so as to gain accuracy is often not an option. In fact, due to the necessary mirroring, this corresponds to a huge growth of the degrees of freedom. Moreover, the use of hyperbolic sparse grids (see [27], for instance) is not possible, since the possibility of discarding coefficients and grid points is given only for fast decaying Fourier coefficients, that is spectral order of convergence to the exact solutions.

The order reduction in Fourier decomposition of the solutions to be approximated and the needed duplication along axes in order to satisfy at least the periodicity of the values of the solutions suggest to explore the alternative of a finite difference discretization in space.

3.2. Time splitting finite difference method

The main advantage of a finite difference approach is that the mirroring of the solution is not required, being the extension of the bounded domain replaced by the imposition of homogeneous Neumann boundary conditions. As shown above, this implies the conservation of the mass over bounded domains.

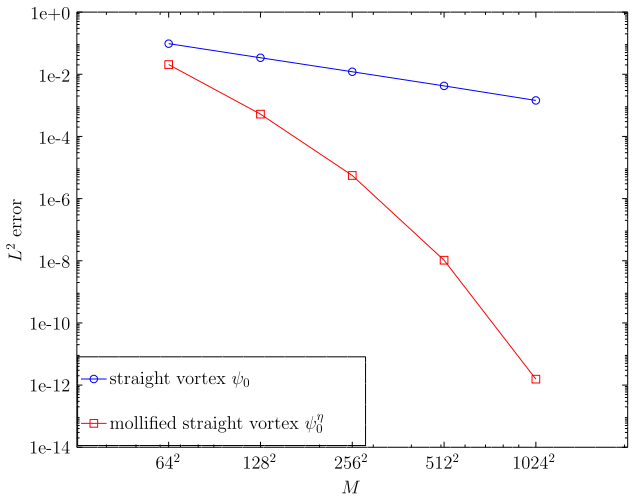

Fig. 3. Error behavior of the Fourier approximation of functions (12) (extended to $[-L, 3L)^2$ by mirroring).

We use centered second order finite differences. With the aim of increasing the spatial resolution around the vortex cores and keeping a reasonable degree of freedom, we employ a set of nonuniform grid points (see [28], for instance, for locally adaptive finite element discretizations).

The discretization of the Laplace operator in one dimension with nonuniform finite differences on m points provides the nonsymmetric matrix

$$A_1 = \begin{bmatrix} -\frac{2}{h_1^2} & \frac{2}{h_1^2} & 0 & \dots & 0 \\ \frac{2}{h_1(h_1+h_2)} & -\frac{2}{h_1 h_2} & \frac{2}{h_2(h_1+h_2)} & \ddots & 0 \\ 0 & \ddots & \ddots & \ddots & 0 \\ 0 & \ddots & \frac{2}{h_{m-2}(h_{m-2}+h_{m-1})} & -\frac{2}{h_{m-2}h_{m-1}} & \frac{2}{h_{m-1}(h_{m-2}+h_{m-1})} \\ 0 & \dots & 0 & \frac{2}{h_{m-1}^2} & -\frac{2}{h_{m-1}^2} \end{bmatrix}$$

where $h_i = x_{i+1} - x_i, x_1 = -L, x_m = L$. This is not exactly a second order approximation, although a discretization in which $h_{i+1} = (1+\delta)h_i$ and a refinement with $h_{j+1} = (1+\delta)^{1/2}h_j$ yields a first order term in the error decaying faster than the second order term (see [29, § 3.3.4]). The approximation for the two-dimensional and the three-dimensional cases can be simply obtained by Kronecker products with the identity matrix. If we call A the corresponding matrix, Eq. (10a) is transformed into the system of ordinary differential equations

$$y'(t) = \frac{\mathrm{i}}{2} A y(t), \quad y(t) \in \mathbb{C}^{M\times 1}. \tag{13}$$

Because of the homogeneous Neumann boundary conditions, we investigate the mass preservation for the numerical solution of system (13). A quadrature formula with positive weights for the computation of the mass writes

$$\int_\Omega |\psi(t,x)|^2 \mathrm{d}x \approx w^T |y(t)|^2, \quad w \in \mathbb{R}_+^{M\times 1}.$$

It can be written as

$$y(t)^* W y(t)$$

where $y(t)^* \in \mathbb{C}^{1\times M}$ denotes the transposed conjugate vector of $y(t)$ and W the matrix with diagonal w. We define $z(t) = W^{1/2} y(t)$ such that

$$z'(t) = \frac{\mathrm{i}}{2} A_w z(t) \tag{14}$$

with $A_w = W^{1/2} A W^{-1/2}$. If A_w is real and *symmetric*, then $\exp(\tau \mathrm{i}/2 A_w)$ is an orthogonal matrix and

$$z(\tau)^* z(\tau) = z^*(0) z(0).$$

This means that

$$y(\tau)^* W y(\tau) = (W^{1/2} y(\tau))^* (W^{1/2} y(\tau)) = z(\tau)^* z(\tau) = z(0)^* z(0) =$$
$$= (W^{1/2} y(0))^* (W^{1/2} y(0)) = y(0)^* W y(0)$$

and therefore system (13) preserves the mass at the discrete level if W makes A_w symmetric. From the structure of the matrix A_1, it is clear that the vector of trapezoidal weights $w^T = [h_1, h_1 + h_2, h_2 + h_3, \ldots, h_{m-1}]$ gives a matrix W_1 such that $W_1 A_1$ is symmetric. The extension to W in the two-dimensional and three-dimensional cases is trivial and this is enough to get A_w symmetric as well, in fact $A^T W = WA \iff W^{-1/2} A^T W = W^{1/2} A \iff W^{-1/2} A^T W^{1/2} = A_w^T = W^{1/2} A W^{-1/2} = A_w$. We conclude that Eq. (13) preserves the mass at the discrete level whenever the trapezoidal rule is used as quadrature formula and this is easily extended to any space dimension.

System (14) could be solved, for instance, by the Crank–Nicolson scheme

$$z_{n+1} = z_n + \frac{k\mathrm{i}}{4} A_w z_n + \frac{k\mathrm{i}}{4} A_w z_{n+1},$$

which preserves the discrete mass being A_w symmetric (see [12]). This scheme is second order accurate in time, therefore the size of the time step k has to be chosen such that the error is smaller than the time splitting error. Moreover, Crank–Nicolson scheme requires the solution of a linear system of equations with matrix $(I - k\mathrm{i}A_w/4)$ at each time step k. Although this is not a big deal in one space dimension, since the matrix is tridiagonal, in higher dimensions the discretization yields a large, sparse, complex symmetric matrix. This implies the use of preconditioned Krylov solvers for general matrices such as GMRES or BiCGStab or minimal residual methods for complex symmetric systems (see [30]). Iterative methods converge to the solution up to a specified tolerance which therefore influences the mass conservation and the whole accuracy of the result. Given these complications, we prefer to consider a direct approximation of the exact solution

$$z_{n+1} = \exp(\tau \mathrm{i}/2 A_w) z_n.$$

Nowadays there are several options for the computation of the action of the matrix exponential to a vector. We refer to [31] for a review of *polynomial* methods which do not require the solution of linear systems. In this way, the kinetic linear part (10a) is solved exactly in time, as in the Fourier spectral method, but usually at a higher computational cost.

4. Numerical experiments

In this section we extensively investigate the accuracy of the methods introduced above by comparing different Padé approximations of the initial solution, uniform versus nonuniform finite differences, and Fourier spectral method versus nonuniform finite differences. We finally assess the upper limit to the maximum accurate resolution of Fourier spectral method and explore the possibility of evaluating a coarse Fourier solution on a fine nonuniform grid.

In Section 2 we have derived various approximations of $\rho(r)$ for a straight, two-dimensional vortex, whose wave function is $\psi(r, \theta) = \sqrt{\rho}\mathrm{e}^{\mathrm{i}\theta}$. In order to quantitatively compare the two methods introduced in Section 3, we measure the preservation of such a steady solution by reporting the relative error

$$\max_{0<|r|\le R} \frac{|\psi_n(r,\theta) - \psi_0(r,\theta)|}{|\psi_0(r,\theta)|}, \quad n = 1, 2, \ldots, T/\tau \tag{15}$$

with $\psi_0(r, \theta) = |\psi_0(r)|\, \mathrm{e}^{\mathrm{i}\theta}$, where $|\psi_0(r)|$ is either $\sqrt{\rho_q(r)}$ or $\sqrt{\rho_{\mathrm{num}}(r)}$, the latter evaluated at any required r by linear interpolation of (8). The origin is excluded since ψ_0 is zero therein. The time step τ is chosen such that T/τ is an integer, where T is the final simulation time. In all our experiments, we selected $T = 10$. The maximum over the continuum set $\{0 < |r| \le R\}$ in the error above is approximated by the maximum over a discrete set which will be specified later.

Although the preservation of the initial state may seem a trivial test, it is in fact a reliable and necessary experiment in order to validate the effectiveness of the proposed numerical methods. Thanks to the reliability of the analytical solution, this test can show the influence of both the spatial approximation and the time splitting error in the numerical discretization of the PDE (1). In this simulation the exact mass over any bounded numerical domain is obviously preserved.

In what follows we will employ either TSSP (Fourier) or TSFD. For a computational grid with $m \times m$ grid points in the physical domain of interest, TSSP requires a total of $M = 2m \times 2m = 4m^2$ degrees of freedom due to mirroring, whereas TSFD requires only $M = m^2$ degrees of freedom thanks to homogeneous Neumann boundary conditions.

4.1. Comparison between different approximations of the initial condition

We preliminarily test the reliability of the three Padé approximations ρ_q, $q = 2, 3, 4$ and the numerical solution of Eq. (7) obtained by central second order finite differences with $N = 5000$ uniformly distributed discretization points. For the solution of the GPE (1) we employ TSSP with Fourier basis functions on a uniform two-dimensional computational grid and 5000 time steps. For this reason, the numerical solution $\tilde{g}(s)$ of Eq. (7) must be interpolated.

Results are reported in Fig. 4, where the relative error defined by (15) is plotted versus time for different disks. The number of Fourier modes is fixed to $m = 2 \cdot 200$, i.e. $M = 1.6 \times 10^5$ degrees of freedom. We compare the solution at each time step with the initial condition on the grid nodes within the considered disk. The worst approximation of the steady-state solution is the commonly used ρ_2 Padé approximation, whereas $\psi_0(r, \theta) = \sqrt{\rho_4(r)}\mathrm{e}^{\mathrm{i}\theta}$ turns out to be as accurate as the numerical solution. For this reason, in the following experiments we will consider only $\psi_0(r, \theta) = \sqrt{\rho_4(r)}\mathrm{e}^{\mathrm{i}\theta}$. All curves collapse on each other in the case of the largest disk, meaning that the maximum error occurs at the boundaries, mainly due to the nonperiodicity of the solution.

4.2. Uniform vs. nonuniform finite differences

We compare the performance of the finite difference approximation on a uniform versus nonuniform grid. The uniform grid has the same step-size h as the grid employed for the Fourier approach and reported in Fig. 4. The nonuniform grid is generated by taking into account different constraints. Given the smallest step-size $h_{\min} = h_1 = 0.05$ at the origin (in the vortex core), we linearly increase the step-size according to $h_{i+1} = (1 + \delta)h_i$ in both x and y and in both positive and negative directions. We choose δ so as to reach the boundaries exactly, and in order to keep the ratio $K = h_{\max}/h_1 \approx 10$, where $h_{\max} = \max h_i$. The number of points of the nonuniform grid

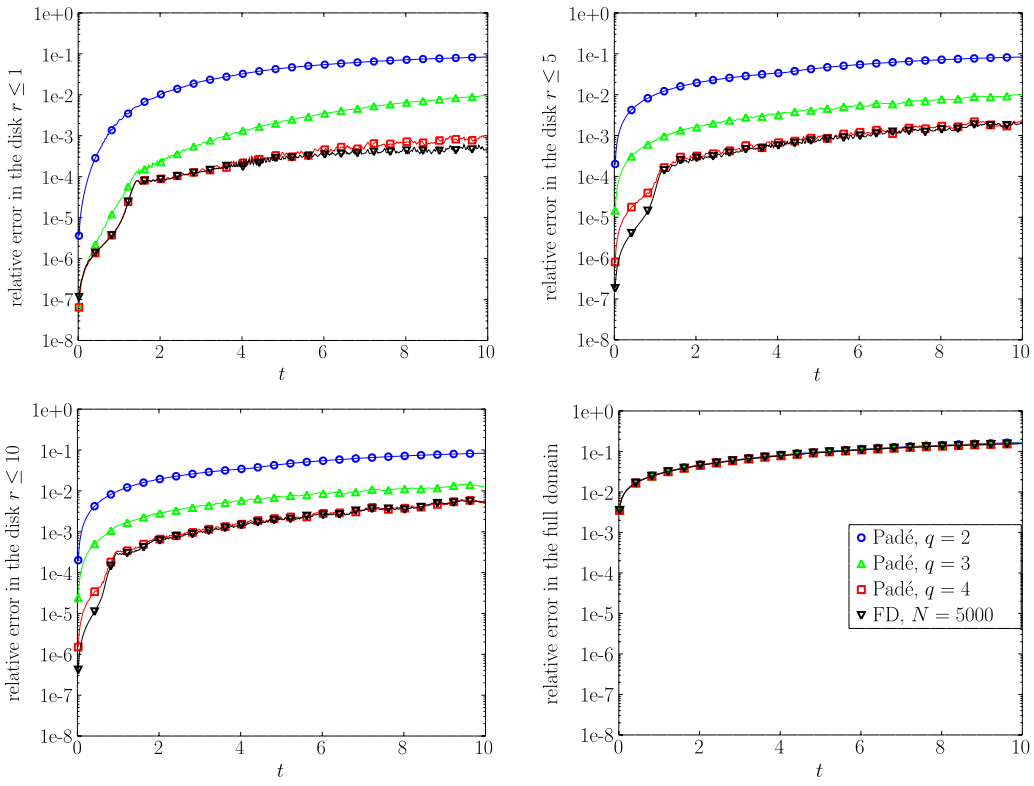

Fig. 4. Comparison of the relative error as defined by (15) for different choices of the initial condition, Fourier approach.

is chosen such that the mean value of $\{h_i\}$ equals the step-size of the uniform grid. These constraints guarantee a reasonable nonuniform grid. The number of time steps is 5000.

The comparison between the uniform and nonuniform grids is shown in Fig. 5. In all cases the initial condition is $\psi_0(r,\theta) = \sqrt{\rho_4(r)}\mathrm{e}^{\mathrm{i}\theta}$, thus the error for the uniform grid can be compared directly with that in Fig. 4 for the case of Padé approximation with $q = 4$ (red squares in both Figures).

We first focus on the results with the same number of points and the same boundaries, i.e. red squares and blue circles in Fig. 5. The discrete mass variation along time integration is comparable and of order 10^{-13}. This confirms the conservation of mass also for the case of nonuniform grid, as discussed in Section 3.2. In the nonuniform case the error is roughly one order of magnitude smaller than in the uniform case on small disks and for t not too large, whereas the curve of the nonuniform case tends to jump onto the uniform one after a certain time as the radius of the disk of interest increases. This suggests the idea that the error arises at the boundaries, where $\psi_0(r,\theta)$ does not exactly fulfill Neumann boundary conditions.

Motivated by this, we have changed the boundaries from $L = 20$ to $L = 30$ and $L = 10$ to check the dependency of the error on the choice of the truncated domain. In doing so, we have preserved the constraints on the nonuniform grids discussed above, obtaining $M = 101^2$ degrees of freedom for $L = 10$ (upward green triangles) and $M = 301^2$ degrees of freedom for $L = 30$ (downward black triangles). With reference to Fig. 5, the domain bounded at $L = 10$ is clearly too small and the error is always very large compared to all the other cases. On the other hand, the curves for $L = 20$ (blue circles) and $L = 30$ (downward black triangles) behave roughly in the same way up to a certain value of t, after which the case $L = 20$ consistently show larger errors than the case $L = 30$. This reinforces the claim that the error arises from the boundary conditions.

4.3. Comparison between Fourier spectral method and nonuniform finite differences

Now we concentrate on our main goal, which is the comparison between TSSP with Fourier basis function on uniform grids and TSFD on a nonuniform grid that we fix to $h_{\min} = 0.05$, $L = 20$, $m = 201$. In order to compare the error defined by (15) for the two methods, we always evaluate the TSSP solution on the nonuniform grid points (spectral solutions can be evaluated everywhere). This set of points has the advantage of being denser in the vortex core, where higher spatial resolution is desirable. Results are reported in Fig. 6, where SP stands for spectral and NFD for nonuniform finite differences.

Keeping in mind that the spectral Fourier approach needs mirroring, i.e. the number of modes in each direction must be doubled, we first choose a number of Fourier modes $m = 2 \cdot 200$ in each direction to make it equal to the number of points of the reference case for nonuniform finite differences ($m = 201$) in the physical (unmirrored) domain. The overall behavior of the error for these two cases is comparable: TSSP (red squares) performs better than TSFD (blue circles) for small values of t, whereas the opposite happens for intermediate values of t. For large t the two curves collapse on each other.

Due to the fact that TSSP needs mirroring, i.e. $M_{\mathrm{TSSP}} = 4M_{\mathrm{TSFD}}$, in Fig. 6 we explore also the cases with less Fourier modes, namely $m = 2 \cdot 100$ (upward green triangles) and $m = 2 \cdot 50$ (downward black triangles). As observed for the case $m = 2 \cdot 200$, in the long term

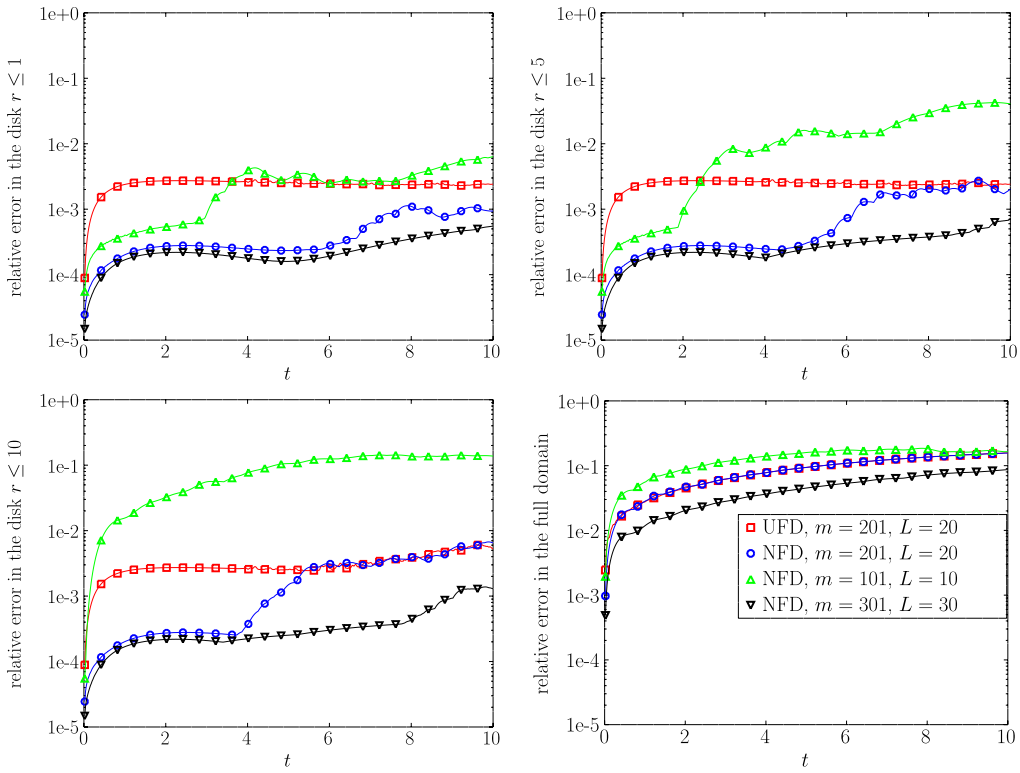

Fig. 5. Comparison of the relative error as defined by (15) for central finite differences on uniform (UFD) and nonuniform (NFD) grids.

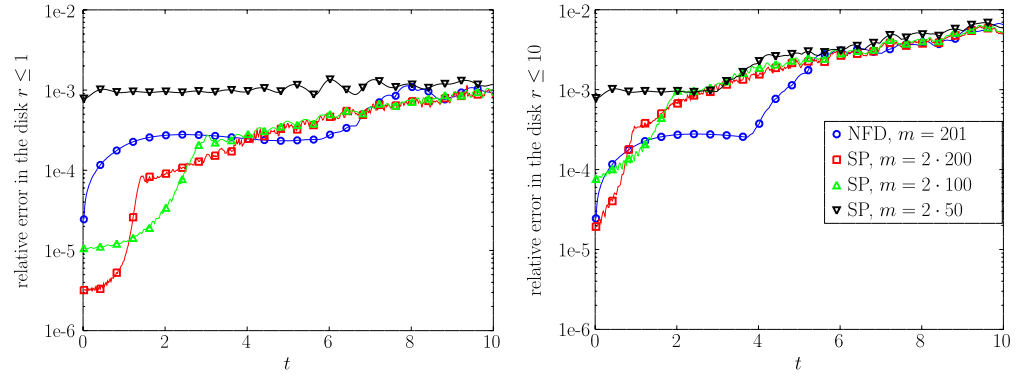

Fig. 6. Comparison of the relative error as defined by (15) between nonuniform finite differences (NFD) and spectral Fourier (SP) for different numbers of Fourier modes.

all curves seem to provide similar errors, regardless of the disk radius. On the other hand, for small values of t, the number of degrees of freedom plays a rôle in that a larger number of Fourier modes ensure smaller errors.

It is important to keep in mind that, for what seen in Fig. 3, the TSSP Fourier approach does not retain the spectral accuracy because of the lack of periodicity at the boundaries.

As a final remark, we observe that the error of the Fourier solution computed on its own uniform grid, reported in Fig. 4 with red squares, is smaller than the error of the Fourier solution evaluated on the nonuniform grid, reported in Fig. 6 with red squares.

4.4. Maximum accurate resolution of Fourier spectral method

As expected, from Fig. 6 we have seen that the smaller the number of Fourier modes, the larger the relative error with respect to the initial condition.

We wish to check if there exists an upper limit to the maximum resolution of Fourier spectral method. For doing so, we increase the number of Fourier modes and, proportionally, the number of time steps as suggested in [32]. Results are shown in Fig. 7. We observe high accuracy in the core (see smaller disk, left plot) for small values of t, immediately followed by saturation. In a larger disk (right plot), saturation kicks in almost immediately. The errors reported in Fig. 7 suggest that $m = 2 \cdot 200$ is a reasonable value of Fourier modes for the preservation of a two-dimensional quantum vortex in a computational domain $[-L, 3L)^2$, $L = 20$. Since the healing length is $\xi = 1$, the grid size is $\xi/5$.

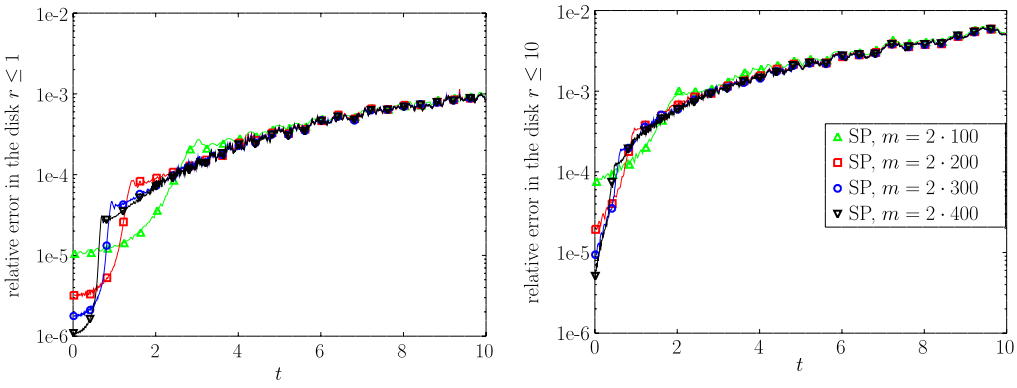

Fig. 7. Comparison of the relative error as defined by (15) for increasing number of Fourier modes.

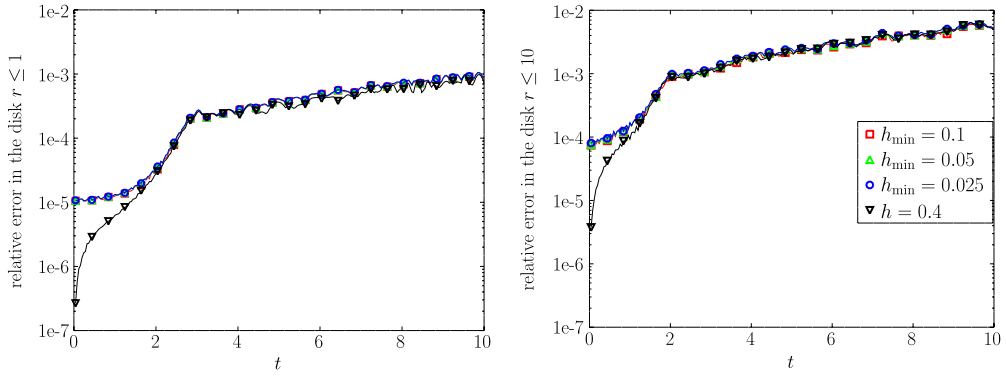

Fig. 8. Comparison of the relative error as defined by (15) for different evaluations of the Fourier solution ($m = 2 \cdot 100$) at nonuniform grids.

4.5. *Fourier evaluation on nonuniform grids*

As explained in the Introduction, our motivation to explore the nonuniform finite difference approach is based on the need of high *local* spatial resolution and accuracy. For instance, this is a challenging requirement for the study of vortex reconnections.

Instead of increasing the number of Fourier modes so as to reach higher *global* spatial resolution, one can resort to a TSSP method with a reasonable number of modes (considering that mirroring is needed) and then evaluate the TSSP solution on a nonuniform grid, with denser points where they are needed. In Fig. 8 we compare the reasonable case $m = 2 \cdot 100$, for which the number of modes is relatively small, but not too small, with different nonuniform grids. We notice that the numerical integration itself is carried out only once and the Fourier coefficients of the solution are stored at each time step. The evaluation at the grid points is performed afterward, in the post processing stage, as many times as desired. Moreover, tools like the Nonuniform Fast Fourier Transform (NFFT, see [33,34]) might be employed for the fast evaluation of trigonometric polynomials at arbitrary point sets. The constant spatial step-size of the TSSP method is $h = 0.4$, whereas $h_{\min}$ stands for the minimum value of the step-size, in the proximity of the origin, for the nonuniform grids. As seen before, there is a substantial difference in the error only for $t < 2$, whereas for larger values of t evaluating the Fourier solution on a nonuniform grid does not worsen the solution. Evaluating a TSSP solution on a locally refined grid is, thus, a very promising approach to study, for instance, quantum vortex reconnections.

5. Conclusions

After deriving a new accurate Padé approximation for the density distribution of a two-dimensional steady-state vortex, we have used it as the initial condition for the Gross–Pitaevskii equation to test the performance of the time-splitting Fourier method. We showed that, although it cannot retain its classical spectral accuracy in space being as accurate as low-order finite difference on nonuniform grids, it preserves quite well the steady-state solution, especially in the neighborhood of the vortex core. Moreover, the Fourier approach is easy to implement and generally fast, thanks to FFT. The additional advantage of a post-processing evaluation on arbitrary points makes this approach suited for applications where *local* high resolution is required.

Appendix. Detailed derivation of Padé approximations

The case $q = 2$. The coefficients of this expansion are already known, however it is instructive to proceed with their derivation in order to understand how it works. We have to compute 3 coefficients, a_1, b_1 and a_2, therefore we can use only 3 equations. These equations are obtained by nullifying, respectively, the coefficients of the terms r^2, r^4 and r^6 in the numerator $N_2(r)$ (lower-order powers of r^{2k}). By nullifying the coefficient of r^2, we get

$$-4a_1^2 b_1 + 4a_1 a_2 + a_1^2 = 0,$$

Table A.1
Coefficients of Padé approximations ρ_2 and ρ_3.

	$q=2$	$q=3$
a_1	$\frac{11}{32}$	0.34003812123694735361
b_1	$\frac{5-32a_1}{48-192a_1}$	$\frac{2304a_1^3+656a_1^2-421a_1-28}{7680a_1^2-1680a_1-330}$
a_2	$a_1\left(b_1-\frac{1}{4}\right)$	$a_1\left(b_1-\frac{1}{4}\right)$
b_2		$\frac{768a_1b_1-120b_1-384a_1^2+8a_1+7}{4608a_1-1152}$
a_3		$\frac{a_1(192b_2-48b_1+16a_1+5)}{192}$

from which $a_2 = a_1\left(b_1 - \frac{1}{4}\right)$. By nullifying the coefficient of r^4, and replacing a_2 with the expression above, we get

$$a_1^2(192a_1b_1 - 48b_1 - 32a_1 + 5) = 0,$$

which gives $b_1 = \frac{5-32a_1}{48-192a_1}$. If we now nullify the coefficient of r^6 and replace a_2 with $a_1\left(b_1 - \frac{1}{4}\right)$ and b_1 with $\frac{5-32a_1}{48-192a_1}$, we get the following equation

$$a_1^2(8a_1 + 1)(32a_1 - 11) = 0.$$

Clearly, $a_1 = 0$ is not acceptable, nor is $a_1 = -\frac{1}{8}$. The only acceptable value is $a_1 = \frac{11}{32}$. As we mentioned before, Eq. (2) cannot be satisfied exactly, however, an *a posteriori* evaluation reveals that the remaining coefficients of r^{2k} are smaller than 1.5×10^{-4} and monotonically decreasing with k.

The case $q = 3$. Since we have to compute 5 coefficients we need 5 equations, which are obtained by imposing that the coefficients of the terms r^2, r^4, r^6, r^8 and r^{10} must be zero. By nullifying the coefficient of r^2 we still get the same equation as for $q = 2$, $-4a_1^2b_1+4a_1a_2+a_1^2 = 0$, from which $a_2 = a_1\left(b_1 - \frac{1}{4}\right)$. By nullifying the coefficient of r^4, and replacing a_2 with the expression above, we get

$$192a_1b_2 - 48a_1b_1 - 192a_3 + 16a_1^2 + 5a_1 = 0,$$

which is easy to solve for a_3 leading to

$$a_3 = \frac{a_1(192b_2 - 48b_1 + 16a_1 + 5)}{192}.$$

Now we collect terms in r^6 and impose its coefficient to be zero. In this equation we replace a_2 and a_3 with the expressions derived above and get the equation

$$4608a_1b_2 - 1152b_2 - 768a_1b_1 + 120b_1 + 384a_1^2 - 8a_1 - 7 = 0,$$

which we solve for b_2:

$$b_2 = \frac{768a_1b_1 - 120b_1 - 384a_1^2 + 8a_1 + 7}{4608a_1 - 1152}.$$

Then we nullify the coefficient of r^8, substitute all previously found a_2, a_3 and b_2, getting the equation

$$7680a_1^2b_1 - 1680a_1b_1 - 330b_1 - 2304a_1^3 - 656a_1^2 + 421a_1 + 28 = 0,$$

which gives

$$b_1 = \frac{2304a_1^3 + 656a_1^2 - 421a_1 - 28}{7680a_1^2 - 1680a_1 - 330}.$$

Finally, we nullify the coefficient of r^{10}, substitute a_2, a_3, b_2 and b_1, and get the equation for a_1

$$a_1^2\left(21233664a_1^5 - 9732096a_1^4 - 62464a_1^3 + 137856a_1^2 + 62772a_1 - 1247\right) = 0.$$

This equation must be solved numerically and leads to many real solutions. However the only value that reproduces a physical behavior of $\rho_3(r)$ for $r \to 0$ is $a_1 = 0.34003812123694735361$. It is possible to compute the first derivative and verify that $\rho_3'(r) > 0$ for all $r > 0$. In other words, ρ_3 is a physical, monotonically increasing, approximation of the density due to a two-dimensional quantum vortex. Again, the coefficients of r^{2k} that are not zero are, indeed, smaller than 4.0×10^{-4} and monotonically decreasing with k. Table A.1 summarizes the coefficients for the cases $q = 2$ and $q = 3$.

The case $q = 4$. Now we have 7 coefficients to compute, therefore we need 7 equations, i.e. we need to nullify the coefficients of r^{2k} for $k = 1, \ldots, 7$. By canceling the term r^2 and solving for a_2 we get the usual expression $a_2 = a_1\left(b_1 - \frac{1}{4}\right)$. By nullifying the term r^4, substituting a_2 and solving for a_3 we get $a_3 = \frac{a_1(192b_2-48b_1+16a_1+5)}{192}$, which is the same expression obtained for ρ_3. By canceling the term r^6, substituting a_2 and a_3 as found, and solving for a_4 we get

$$a_4 = \frac{4608a_1b_3 - 1152a_1b_2 + (384a_1^2 + 120a_1)b_1 - 128a_1^2 - 7a_1}{4608}.$$

Table A.2
Coefficients of Padé approximation ρ_4.

	$q = 4$
a_1	0.34010790700196714760
b_1	$\frac{2304a_1^3+656a_1^2-421a_1-28}{7680a_1^2-1680a_1-330}$
a_2	$a_1\left(b_1-\frac{1}{4}\right)$
b_2	$\frac{(737280a_1^3+209920a_1^2-134720a_1-8960)b_1-364544a_1^3+70144a_1^2+18256a_1+393}{2457600a_1^2-537600a_1-105600}$
a_3	$\frac{a_1(192b_2-48b_1+16a_1+5)}{192}$
b_3	$\frac{(61440a_1-9600)b_2+(-30720a_1^2+640a_1+560)b_1+8448a_1^2-1056a_1-21}{368640a_1-92160}$
a_4	$\frac{4608a_1b_3-1152a_1b_2+(384a_1^2+120a_1)b_1-128a_1^2-7a_1}{4608}$

By canceling the term r^8, substituting a_2, a_3, a_4 and solving for b_3 we get

$$b_3 = \frac{(61440a_1 - 9600)b_2 + (-30720a_1^2 + 640a_1 + 560)b_1 + 8448a_1^2 - 1056a_1 - 21}{368640a_1 - 92160}.$$

By canceling the term r^{10}, substituting a_2, a_3, a_4 and b_3, and solving for b_2 we get

$$b_2 = \frac{(737280a_1^3 + 209920a_1^2 - 134720a_1 - 8960)b_1 - 364544a_1^3 + 70144a_1^2 + 18256a_1 + 393}{2457600a_1^2 - 537600a_1 - 105600}.$$

By canceling the term r^{12}, substituting all known a_j, b_3, b_2, and solving for b_1 we get

$$b_1 = \frac{722731008a_1^5 - 326467584a_1^4 - 13427712a_1^3 + 11551104a_1^2 + 834006a_1 - 12183}{2972712960a_1^5 - 1362493440a_1^4 - 8744960a_1^3 + 19299840a_1^2 + 8788080a_1 - 174580}$$

Finally by canceling the term r^{14}, substituting all a_j, b_k previously found, we get an equation for a_1

$$\begin{aligned}&1292033536819200a_1^8 - 2530164294549504a_1^7 + 1853440540016640a_1^6 - \\ &642522859438080a_1^5 + 107808283328512a_1^4 - 8028170208256a_1^3 + \\ &248539665024a_1^2 + 1297120628a_1 + 9325957 = 0.\end{aligned}$$

This equation has many real solutions, which can be determined numerically. However, the only value that leads to a physically acceptable $\rho_4(r)$ for $r \to 0$ is $a_1 = 0.34010790700196714760$. After computing all other coefficients and the first derivative, it is straightforward to verify that $\rho_4'(r) > 0$ for all $r > 0$, i.e. ρ_4 is a physical, monotonically increasing, approximation of the density for a two-dimensional quantum vortex. As observed before, the coefficients of r^{2k} that are not zero are smaller than 1.9×10^{-11} and monotonically decreasing with k. Table A.2 summarizes the coefficients for the case $q = 4$.

References

[1] W.F. Vinen, Phil. Trans. R. Soc. A 366 (2008) 2925–2933.
[2] M.S. Paoletti, D.P. Lathrop, Ann. Rev. Cond. Mat. Phys. 2 (2011) 213–234.
[3] C.F. Barenghi, L. Skrbek, K.R. Sreenivasan, Proc. Natl. Acad. Sci. USA 111 (2014) 4647–4652.
[4] U. Frisch, Turbulence, Cambridge University Press, Cambridge, England, 1995.
[5] S.B. Pope, Turbulent Flows, Cambridge University Press, Cambridge, England, 2000.
[6] F. Hussain, K. Duraisamy, Phys. Fluids 23 (2011) 021701(4).
[7] S. Zuccher, M. Caliari, A.W. Baggaley, C.F. Barenghi, Phys. Fluids 24 (2012) 1–21.
[8] L.P. Pitaevskii, Sov. Phys.—JETP 13 (1961) 451–454.
[9] E.P. Gross, J. Math. Phys. 4 (1963) 195–207.
[10] P.H. Roberts, N.G. Berloff, in: C.F. Barenghi, R.J. Donnelly, W.F. Vinen (Eds.), Quantized Vortex Dynamics and Superfluid Turbulence, in: Lecture Notes in Physics, vol. 571, Springer Berlin Heidelberg, 2001, pp. 235–257.
[11] N.G. Berloff, J. Phys. A: Math. Gen. 37 (2004) 1617–1632.
[12] W. Bao, Y. Cai, Kinet. Relat. Models 6 (2013) 1–135.
[13] S. Zuccher, R.L. Ricca, Phys. Rev. E 92 (2015) 061001.
[14] L. Kondaurova, V. L'vov, A. Pomyalov, I. Procaccia, Phys. Rev. B 89 (2014) 014502.
[15] M.D. Bustamante, R.M. Kerr, Physica D 237 (2008) 1912–1920.
[16] R. Hänninen, A.W. Baggaley, Proc. Natl. Acad. Sci. USA 111 (2014) 4667–4674.
[17] J. Koplik, H. Levine, Phys. Rev. Lett. 71 (1993) 1375–1379.
[18] A.J. Allen, S. Zuccher, M. Caliari, N.P. Proukakis, N.G. Parker, C.F. Barenghi, Phis. Rev. A 90 (2014) 013601.
[19] S. Zuccher, R.L. Ricca, Phys. Rev. E 95 (2017) 053109.
[20] M.W. Scheeler, D. Kleckner, D. Proment, G.L. Kindlmann, W.T.M. Irvine, Proc. Natl. Acad. Sci. USA 111 (2014) 15350–15355.
[21] A. Villois, G. Krstulovic, D. Proment, H. Salman, J. Phys. A 49 (2016) 415502.
[22] C. Rorai, J. Skipper, R.M. Kerr, K.R. Sreenivasan, J. Fluid Mech. 808 (2016) 641–667.
[23] A. Villois, D. Proment, G. Krstulovic, Phys. Rev. Fluids 2 (2017) 044701.
[24] S. Nazarenko, R. West, J. Low Temp. Phys. 132 (2003) 1–10.

[25] M. Thalhammer, M. Caliari, C. Neuhauser, J. Comput. Phys. 228 (2009) 822–832.
[26] T.P. Billam, M.T. Reeves, B.P. Anderson, A.S. Bradley, Phys. Rev. Lett. 112 (2014) 145301.
[27] V. Gradinaru, SIAM J. Numer. Anal. 46 (2007) 103–123.
[28] M. Thalhammer, J. Abhau, J. Comput. Phys. 231 (2012) 6665–6681.
[29] J.H. Ferziger, M. Perić, Computational Methods for Fluid Dynamics, third ed., Springer, 2002.
[30] S.-C.T. Choi, Tech. Rep. ANL/MCS-P3028-0812, Computation Institute, University of Chicago, Chicago, Illinois, 2013.
[31] M. Caliari, P. Kandolf, A. Ostermann, S. Rainer, BIT 54 (2014) 113–128.
[32] W. Bao, S. Jin, P.A. Markowich, J. Comput. Phys. 175 (2002) 487–524.
[33] J. Keiner, S. Kunis, D. Potts, ACM Trans. Math. Software 36 (2009) 19:1–19:30.
[34] M. Caliari, S. Zuccher, Comput. Phys. Comm. 213 (2017) 197–207.